Sizing of Conceptual Hypersonic Long-Range Transport Aircraft using a Multi-Disciplinary Optimisation Strategy

Thibault Clar [a] Prof. Fabrizio Oliviero [a] Prof. Dries Verstraete [b]

[a] *Delft University of Technology, The Netherlands*

[b] *University of Sydney, Australia*

Abstract

This paper describes the implementation of a conceptual hypersonic transport sizing platform. The platform is based on a Multi-Disciplinary approach aimed at providing rapid evaluation of complete aircraft mass subject to fuel and height requirement constrains. Through the implementation of a parametric aircraft model, automatic geometry (using MIT' Engineering SketchPAD [6]) and mesh (SALOME platform [2]) generators as well as the integration of invicid subsonic (Boeing' PANAIR code [20]) and hypersonic flow solvers (Hypersonic Engineering Methods) with the viscous layer estimations of Eckert, Van Dries and Spalding and Chi, full wing-body aero-thermal characteristics of a arbitrary configuration can be analysed. An efficient Multi-Discipline Feasible strategy based on the GHAME engine performance model [16], thermal protection system parametric curves and empirical based mass relation allow for a consistent conceptual component and fuel mass estimation of the complete configuration. A study on Reaction Engine' LAPCAT A2 conceptual configuration has shown the ability of the current platform to optimally size a hypersonic transport aircraft for varying mission profiles including changes in range and cruise mach number.

Key words: Hypersonic, Multi-Disciplinary Optimisation, Thermal Protection System, Mass estimation, Liquid hydrogen.

1 Introduction

Hypersonic flight, characterised by mach numbers exceeding 3, has been a subject of extensive research since its first appearance in 1949 with the first flight of the V2 rocket. Since this first achievement, a significant number of projects have seen the light over the last 60 years to investigate the challenges and potential of high-speed controlled re-usable flights. Up until recently, most controlled hypersonic aircraft research have been aimed at short acceleration mission such as for the X-15 aircraft or for re-entry vehicles such as the well know Space Shuttle. However, with the ever growing global passenger traffic and the strong acceleration of long haul operations over the last five years, a new potential market has opened for long distance passenger hypersonic flight [21] [14]. Currently, long-range aircraft are close to pushing the limit of what can be achieved in a subsonic regime but will never be capable of providing the significant flight time reductions of hypersonic flight.

Promising development in the field of hypersonic transport vehicles include the liquid hydrogen powered LAPCAT A2 airliner concept which aims to reduce intercontinental flight between Europe and Asia Pacific from 16 to only 4 hours by flying at a cruise mach number of 5 while carrying a payload of 300 passengers [17] [21]. While the potential of using high performance liquid hydrogen propulsion and the reduction in flight times are attractive [25] [10], hypersonic flights present numerous challenges that must be considered early in the vehicle design to successfully understand and predict the performance of such vehicles.

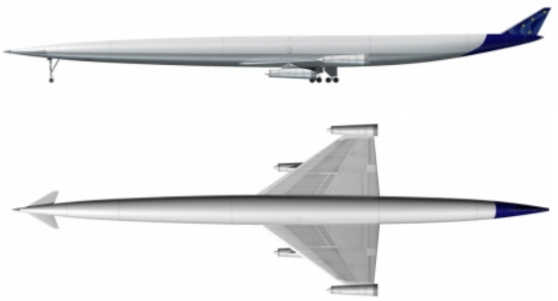

Fig. 1. The LAPCAT A2 conceptual design

In the hypersonic regime the presence of extreme aerodynamic heating, the formation of shocks over the vehicle surface, the low achievable lift to drag ratios [8] and the interactions of such aspects on the vehicle structural and fuel mass call for the use of Multi-Disciplinary Optimisation techniques for the appropriate design of such vehicles. As a result, a Multi-Disciplinary platform has been developed in this study in an effort to capture the interaction among relevant disciplines and to optimally size hypersonic cruise vehicles at a conceptual phase.

In this research, the developed Multi-Disciplinary platform is employed using the LAPCAT A2 conceptual shape and mission as a baseline to first investigate the effects and sensitivity of vehicle shape parameters on the aerodynamic and mass performance of an hypersonic cruise vehicle over a long range mission. An optimisation algorithm is further employed on the LAPCAT A2 baseline configuration to study the potential gains in performance for such an aircraft. The effects of the mission mach number and range on optimal vehicle size are investigated.

2 Model

When considering the design of a hypersonic aircraft, numerous disciplines must be taken into account. Each of these individual disciple have an effect on the other and to adequately capture design sensitivities, the multi-discplinary platform must take into consideration the dependencies of among all disciplines. In the current research, the displines shown in green in figure 2 have been implemented in the developed platform.

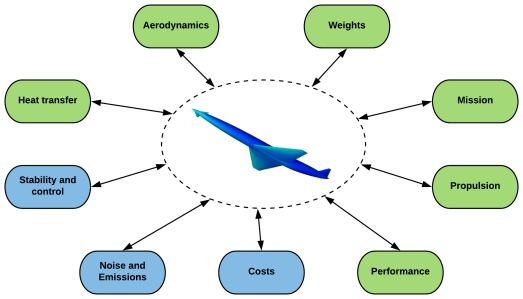

Fig. 2. Main disciplines involved in Hypersonic cruise aircraft design

The Multi-Disciplinary strategy employed in this platform is depicted in figure 3. The vehicle normalised gross take-off mass W_{TO} (with respect to the baseline configuration) for a given mission profile is used as the performance index as it is strongly related to development cost and overall aircraft performance [23]. In this study, the design variables are normalised shape variable which control both the wing platform and the fuselage geometry. The optimal sizing problem design space is bounded by two non-linear constrains. Firstly, the fuel volume available in the fuselage geometry is constrained to accommodate the liquid hydrogen fuel required for the aircraft mission. Secondly, the fuselage passenger cabin height is constrained to a minimum height of 2.5 meters ($H_{cylinder,\min}$) to allow passengers to stand in the cabin. The optimisation problem is formally expressed according to equation 1.

$$
\begin{aligned}
\underset{\vec{X}}{minimise}: \qquad & J_{norm}\left(\vec{X}\right) = \frac{W_{TO}\left(\vec{X}\right)}{W_{TO}\left(\vec{X}_0\right)} \\
st: \qquad & c_{1,norm}\left(\vec{X}\right) = \frac{V_{F,AV}\left(\vec{X}\right) - V_{F,req}\left(\vec{X}\right)}{V_{F,AV}\left(\vec{X}_0\right) - V_{F,req}\left(\vec{X}_0\right)} \leq 0 \\
& c_{2,norm}\left(\vec{X}\right) = \frac{H_{cylinder,fus}\left(\vec{X}\right) - H_{cylinder,\min}}{H_{cylinder,fus}\left(\vec{X}_0\right) - H_{cylinder,\min}} \leq 0
\end{aligned}
\tag{1}
$$

The fundamental working principle of the platform as depicted in the Design Structure Matrix given in figure 3, is to find the combination of shape variables which minimise the objective function subjected to the non-linear constrains imposed. To achieve this, given a constant discretised mission profile, for each new design vector imposed, a new aircraft geometry is generated and meshed. Sub-sequentially, an aero-thermal performance matrix A is created containing the aerodynamic lift and drag polars as well as the heat transfer over the geometry as a function of the angle of attack for each of the discretised mission points. This performance matrix is then used as an input to a Multi-Discipline Feasible (MDF) loop to estimate the aircrat take off mass. The MDF loop ensures consistency among the mission performance, thermal protection sizing and mass estimation modules to converge to an estimated take-off mass value $W_{to,conv}$.

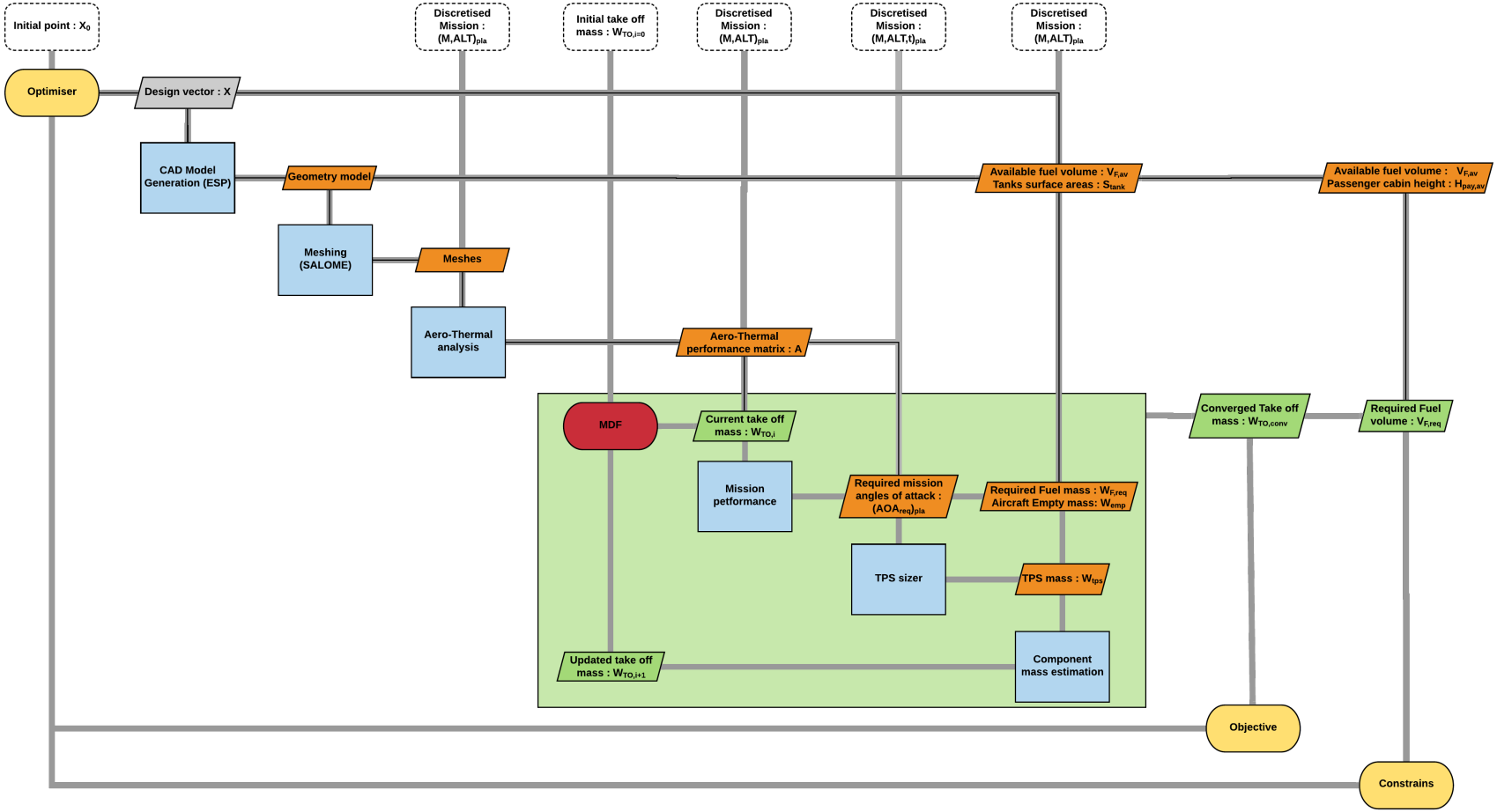

Fig. 3. Design Structure Matrix of MDO platform

2.1 *Aircraft parametric representation and Geometry generation*

Each aircraft model is defined as a set of cross sections provided by the user in a parametric input file. The geometry cross sections are defined using the Class Shape Transformation function for the wing and Super-ellipses for the fuselage. Additionally, the relative positioning of the wing section are defined with respect to a set of planform parameters (see figure 4). This parametric representation of the aircraft allows the generation of a large set of potential candidate geometries.

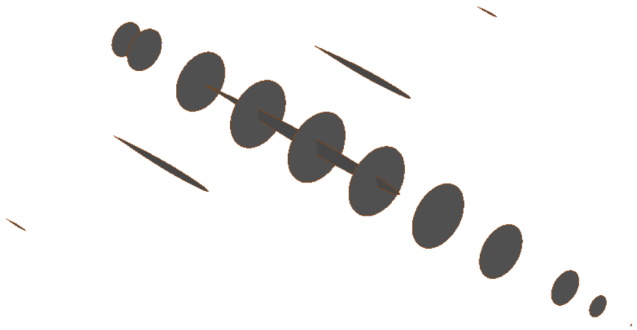

Fig. 4. Example of parametrised fuselage and wing cross sections.

Using the parametric definition of the aircraft, a three dimensional model is automatically generated using the CAD software *Engineering SketchPAD* (ESP) programming interface developed by MIT [5]. This software allows for the rapid generation of three dimensional water-tight geometries as shown in figure 5 and is therefore well suited for this application.

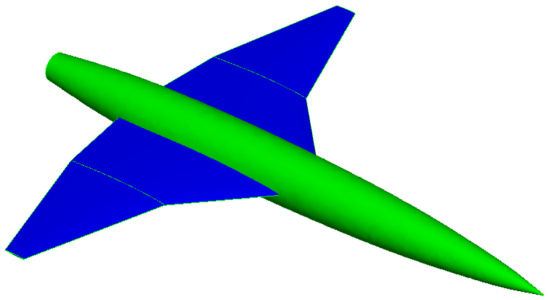

Fig. 5. Fused water-tight aircraft geometry using Engineering SketchPad.

2.2 *Automatic Meshing*

To generate the computational grid required for subsequent aero-thermal analysis of a given geometry, the Open-Source software SALOME [2] is employed. The geometry generated by ESP (Boundary Rrepresentation file) is imported into SALOME and automatically partitioned to construct a set of structured mesh networks as shown in figure 6. In addition, wake networks are generated at the trailling edges of the wing and fuselage for aerodynamic analysis.

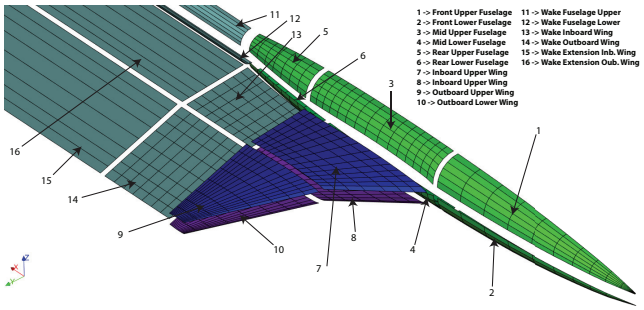

Fig. 6. Exploded view of aircraft mesh networks generated in SALOME platform.

2.3 *Aero-Thermal Analysis*

The Aero-Thermal discipline aims at generating a performance matrix A which contains the lift and drag polar characteristics as well as the heat transfer over the vehicle surface as a function of the angle of attack for each discretised mission point as represented by equation 2. The aircraft mission is an input to the platform and is discretised as a set of plateaux (as shown in figures 7 and 8) from which aero-thermal analysis are performed.

$$A = \begin{bmatrix} C_L(\alpha)_{(M)_{pla_1}} & C_D(\alpha)_{(M,ALT)_{pla_1}} & q(\alpha)_{(M,ALT)_{pla_1}} \\ C_L(\alpha)_{(M)_{pla_2}} & C_D(\alpha)_{(M,ALT)_{pla_2}} & q(\alpha)_{(M,ALT)_{pla_2}} \\ \vdots & \vdots & \vdots \\ C_L(\alpha)_{(M)_{pla_N}} & C_D(\alpha)_{(M,ALT)_{pla_N}} & q(\alpha)_{(M,ALT)_{pla_N}} \end{bmatrix} \quad (2)$$

2.3.1 *Invicid aerodynamic analyses*

At each of the defined mission plateaux, using the meshes generated in SALOME, invicid aerodynamic analysis are performed over a range of angles of attack for both subsonic and supersonic-hypersonic flight conditions by means of panel codes. While panel codes may not be as accurate as solutions provided by CFD analyses, they are capable of quickly estimating aerodynamic performance of a complete configuration making them applicable in an MDO framework. In this analysis, the invicid and viscous computations are decoupled from one another. The viscous and thermal heat transfer calculations use the information regarding the flow properties in the invicid layer to estimate the local properties within the viscous layer using semi-empirical

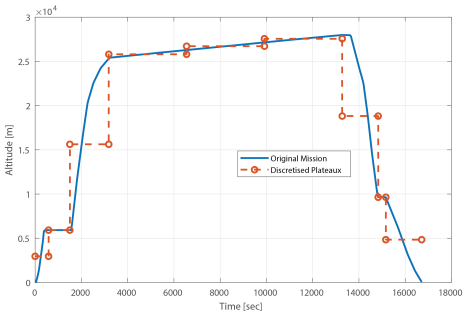

Fig. 7. Discretisation of altitude from original mission.

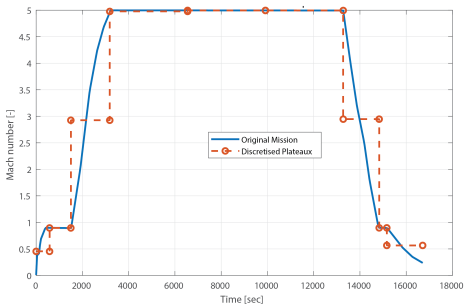

Fig. 8. Discretisation of mach number from original mission.

engineering methods.

Subsonic Aerodynamics:

The subsonic analysis is carried out for each mission plateau defined with $M < 1$. The well known higher order panel code PANAIR developed by Boeing [12] has been implemented for this purpose. This panel code is based on the linearization of the steady-linear potential flow equation to arrive at the Prandlt-Glauert equation.

In the implementation of the PANAIR code, the PANIN pre-processor [18] is used to generate the required input file. To use the PANIN pre-processor, the Langley Wireframe Geometry Standard (LaWGS) format is required to describe the mesh networks with the appropriate boundary conditions applied. In figure 9 and table 1, the geometry network groups described in the LaWGS format and the applied boundary conditions applied are given.

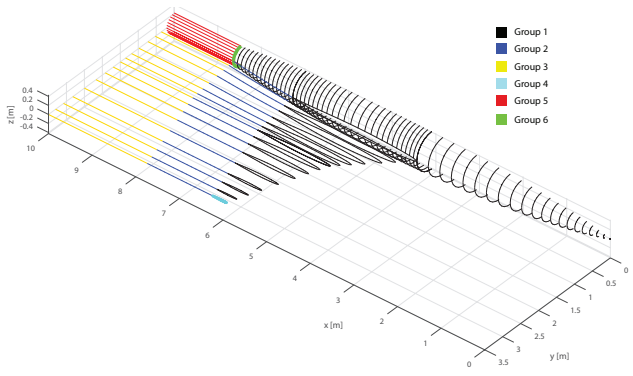

Fig. 9. Wireframe model according to LaWGS format and mesh network groups for boundary conditions.

Table 1
PANAIR boundary condition applied to the different mesh network groups

Mesh Group	Mesh network(s)	Description	PANAIR boundary condition
1	Fuselage (Front, Mid, Rear) Wing (top, bottom)	Direct condition on an impermeable thick surface	8
2	Wing wakes	Vorticity matching kutta condition	18
3	Wing extension wakes	Doublet matching condition	18 (matchw = 1)
4	Wing tip	Direct condition on an impermeable thick surface	8
5	Fuselage body wakes	Doublet matching condition	18 (matchw = 1)
6	Fuselage base	Base surface condition	5

From the output of the panair analysis, the pressure coefficient, velocity perturbations over the surface mesh are obtained as well as the invicid lift and drag polars.

Supersonic-Hypersonic Aerodynamics:

For the plateaux in the supersonic-hypersonic regime ($M >> 1$), the well known supersonic-hypersonic engineering impact-expansion methods are utilised. In these methods, the geometry is analysed along mesh strips whereby the local panel inclination use the hypersonic flow solution of a wedge or cone with equivalent wedge or cone-semi apex angle. From an extensive validation process, the Taylor Maccoll Tangent Cone method [11] is chosen for the fuselage body while the inclined wedge method [3] is applied to the wing surfaces. For panels with negative inclination with respect to the freestream (shadow flow), the expansion flow is modelled using the Prandlt Meyer expansion fan about the previous strip panel as shown in figure 10.

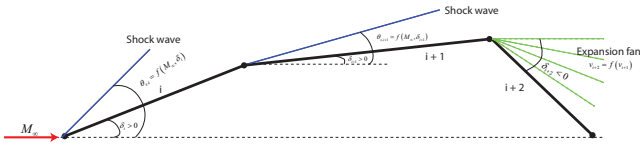

Fig. 10. Impact and shadow flow along mesh strips.

While hypersonic engineering methods are not as accurate as the results that could be obtained using CFD, they have been widely used for the preliminary design of hypersonic vehicles [22] [9]. Although expected to be

small in hypersonic flow, the method bases itself on a component build up approach and thus does not consider possible interference effects.

2.3.2 Viscous-Thermal analysis

To estimate the properties of the flow within the viscous layer, the semi-empirical methods of Spalding and Chi, Eckert and Van Dries [22] have been implemented. These methods use the flow properties of the invicid layer (obtained from the previous analyses) to estimate conditions in the boundary layer and compute the local friction coefficient and heat transfer over the mesh panels. The semi-empirical relations are capable of estimating the local panel friction coefficient through the use of different compressibility correction factors on a flat plate and convective heat transfer to the surface is estimated using equation 3.

$$\dot{q}_{conv} = \rho_{inv} V_{inv} \frac{R_f c_f}{2} \left(c_{spe,aw} T_{aw} - c_{spe_{,w}} T_w \right) \quad (3)$$

Since the local friction and convective heat transfer are dependent on the surface wall temperature, a convective-radiation heat balance $q_{conv} = q_{rad}$ is assumed at the surface and an iterative process is used to solve the non-linear equation given by equation 4 to compute the viscous flow over the configuration.

$$T_{w,i} = \left(\frac{q_{conv,T_{i-1}}}{\varepsilon \sigma} + T_\infty^4 \right)^{1/4} \quad (4)$$

The heat transfer fields obtained over the surface are sub-sequentially interpolated as a function of angle of attack using the Proper Orthogonal Decomposition (POD) method [19] [13] at each mission plateau defined. Using the POD method, the heat transfer fields sampled over the range of angle of attacks for a given plateau are decomposed into a set of independent linear basis functions ϕ_m (modes) scaled by a set of coefficients k_m. The scaling coefficients are furthermore interpolated over the sampled angles of attack to provide a function for the convective heat transfer over the entire configuration for each mission plateau according to equation 5.

$$q_{conv}(\alpha)_{(M,ALT)_{pla}} = \left(\sum_{m=1}^{M} \vec{\phi}_{\lambda_m} k_m(\alpha) \right)_{(M,ALT)_{pla}} \quad (5)$$

Finally the lift and drag polars are added to the performance matrix A through the interpolation of the lift and drag polars obtained at each mission plateau according to equations 6 and 7 where $C_{D,visc}$ is obtained from the viscous-thermal analysis presented in this section.

$$C_L(\alpha)_{(M)_{pla}} = \left[C_{L,\alpha=0} + \frac{dC_L}{d\alpha} \alpha \right]_{(M)_{pla}} \quad (6)$$

$$C_D(\alpha)_{(M,ALT)_{pla}} = \left[C_{D,visc} + C_{D,wave} + k_1 C_L + k_2 C_L^2 \right]_{(M,ALT)_{pla}} \quad (7)$$

2.4 Multi-Discipline Feasible loop

The MDF loop consists of three main modules which are inter-dependent and need to be iteratively evaluated to obtain consistency across the disciplines for a given aircraft shape. The aim of the MDF loop is to obtain a converged value for the estimated take-off mass of the vehicle such that the mass obtained between two iteration is lower than a specified tolerance value $|W_{TO,i+1} - W_{TO,i}| < \Delta_{MDF}$. In order to start the iteration loop, the MDF scheme takes as input the performance matrix A from the aero-thermal analysis and an initial (estimated) take off mass $W_{to,0}$.

2.4.1 Mission Performance

This module takes an estimated take off mass as input. Using the steady flight assumption, the performance matrix A and the discretised mission, the module outputs the angles of attack required throughout the mission plateaux. In addition, the aircraft drag and thrust required are obtained from the required required angles of attacks.

The second output of the performance module is an estimation of the total fuel mass required to fly the given mission. To achieve this, the current platform makes use of the Generic Hypersonic Aerodynamics Model Example (GHAME) Engine developed by White et al. [16] [15]. The GHAME engine assumes a liquid hydrogen propulsion system and has been developed to capture the entire flight envelope of a generic hypersonic vehicle. The module assumes automatic and ideal switch one thermodynamic cycle to the next and provides a model of the engine specific impulse as a function of freestream mach number and angle of attack such that $ISP = f(M, \alpha)$ as shown in figure 11.

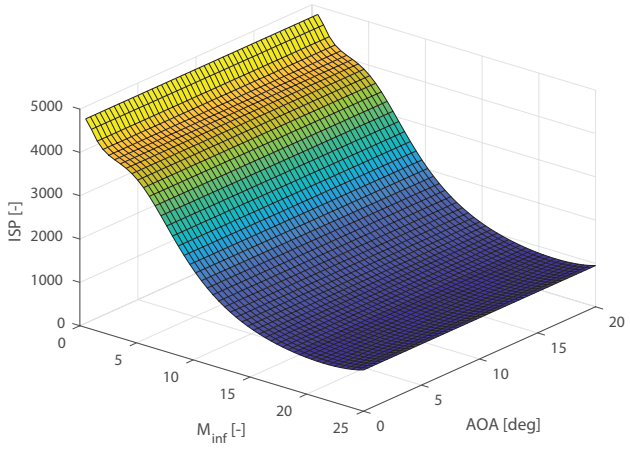

Fig. 11. GHAME engine specific impulse.

From the thrust required at each mission plateau, the fuel mass flow is calculated using the engine model using equation 8. Finally the fuel required for the entire mission is computed using equation 9.

$$\left(\frac{dW_f}{dt}\right)_{pla,i} = \frac{T_{req_{pla,i}}}{g \cdot ISP_{pla,i}} \tag{8}$$

$$W_f = \sum_{i=1}^{N_{pla}} \left[\left(\frac{dW_f}{dt}\right)_{pla,i} (t_{start} - t_{end})_{pla,i}\right] \tag{9}$$

2.4.2 Thermal Protection System sizing

Overall the TPS is sized according to the total convective heat accumulated at each panel during the mission to provide W_{tps}. It has been developed to provide a rapid mass estimation of the TPS while still capturing the effects of changes in local convective heat transfer over the vehicle.

The method used in this platform is adapted from a parametric study from NASA on metallic and ceramic based protection systems [1] which correlates the unit mass for a passive thermal protection system to the total heat load applied. The passive TPS system is often recommended over active and semi-passive concepts for hypersonic transport type vehicles [17] as they are completely reusable and do not required complex active cooling.

The 1D unsteady heat equation is used on a set of different potential TPS materials to derive parametric equations relating tps unit mass to the total heat load applied. To derive these parametric curves, a discretised finite difference scheme (shown in figure 12) is used to solve the unsteady heat equation $\frac{\partial T}{\partial t} = \tau \frac{\partial^2 T}{\partial x^2}$ subject to a convection-radiation-conduction heat balance at the surface and an adiabatic back wall condition as given by equations 10 annd 11. The adiabatic back wall condition is regularly used to model passive TPS as it assumes that no heat is transferred to the substructure.

$$q_{conv} - \varepsilon\sigma\left(T_w^4 - T_\infty^4\right) + k_{mat}\frac{dT}{dx} = 0 \tag{10}$$

$$\frac{dT}{dx} = 0 \tag{11}$$

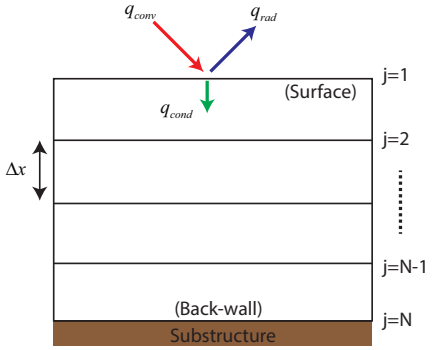

Fig. 12. Schematic of numerical model for TPS.

The parametric unit mass curves have been determined in the platform by minimising the tps unit mass subject to a maximum allowed back wall temperature $T_{BW,max}$ (equation 12) for varying heat flux profiles (figure 13) representative of a typical hypersonic missions.

$$\begin{aligned} &\underset{t_{tps,norm}}{minimise}: \quad J\left(t_{tps,norm}\right) = \frac{W_{unit,tps}(t_{tps,norm})}{W_{unit,ref}} \\ &st: \quad c_{1,norm} = \frac{T_{BW,\max} - T_{BW}}{T_{BW,ref}} < 0 \end{aligned} \tag{12}$$

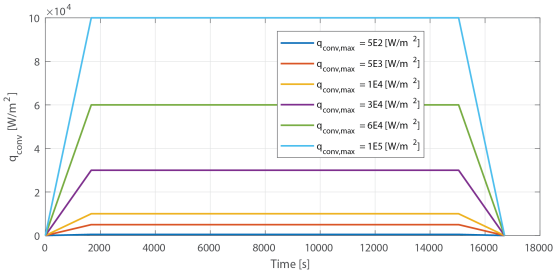

Fig. 13. Heat profiles for TPS unit mass sizing.

The result obtained are parametric curves relating the unit mass of the TPS to the total heat load (integrated

heat flux) for different candidate TPS materials. An example of these parametric curves for four different ceramic based materials constrained to a back wall temperature of 400 Kelvin is provided in figure 14.

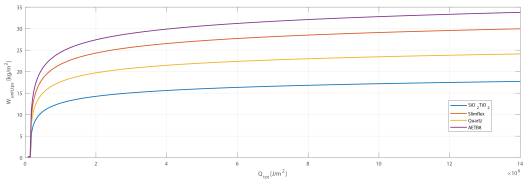

Fig. 14. Unit mass of different tps materials as a function of heat loading at 400 Kelvin back wall temperature ($T_{inf} = 220[K]$).

In the optimisation platform, the parametric curves obtained from the previous analysis are used to estimate the total tps mass over the vehicle during a mission. Using the required angle of attack (at each plateau) obtained from the mission performance module and the POD interpolated heat transfer fields from the aerothermal performance matrix A, the total heat load over each mesh panel P is obtained from equation 13.

$$Q_{tot,P} = \sum_{i=1}^{N_{pla}} \left[q_{conv,pla,i_P} \left(\alpha_{req,pla,i} \right) \cdot \left(t_{start} - t_{end} \right)_{pla,i} \right] \tag{13}$$

Finally the TPS mass over each panel is estimated by evaluating the parametric unit mass function for the panel heat load, multiplied by the panel area. The total TPS mass is then estimated by summing the individual panel tps mass as given in equation 14. The parametric approach to TPS sizing implemented in this platform provides a rapid evaluation of the TPS mass over the entire vehicle which is capable of capturing the effects of changes in vehicle shape and flow conditions.

$$W_{tot,tps} = \sum_{P} \left[f\left(Q_{tot,P} \right) \cdot A_P \right] \tag{14}$$

2.4.3 Mass estimation

This module uses empirical based relations from the Hypersonic Aerospace Sizing Analysis (HASA) [7] and Weight Analysis of Advanced Transport systems (WAATs) [4] methods to estimate the take-off mass and absolute mass of the different aircraft components such as aerodynamic surfaces, fuselage, fuel tanks and subsystems masses. The component empirical relations are mostly based on the geometry of the aircraft and the take-off mass. The sizing methods of HASA and WAATs are applicable to single-stage and two-stage-to-orbit hypersonic aircraft which ensures their applicability to the current platform and the equation from HASA predict a $\pm 10\%$ accuracy in estimated take off mass for a hypersonic vehicle [7].

The HASA and WAATs mass estimation models are both based on an iterative process whereby the take off mass is iteratively determined until a converged mass is obtained. To start the iteration process, the empty mass W_{emp} and fuel mass W_F obtained from the mission performance module are used to set the initial take off mass at iteration 1 such that $W_{TO,j=1} = W_{emp} + W_F$ whereby the fuel mass W_F remains fixed during the mass estimation iteration process. A convergence criteria of 0.1 kg is used for the mass estimation module. Upon convergence of the mass estimation module a new estimated take-off mass value $W_{TO,i+1}$ is obtained and fed back to the MDF loop until consistency among the MDF disciplines is achieved.

3 Case Study

To investigate the ability of the developed platform to optimally size hypersonic transport aircraft vehicles, the Reaction Engines' LAPCAT A2 baseline configuration [21] has been selected with the baseline antipodal 18771 km range mission defined in figures 7 and 8. To achieve this, the optimisation problem formulated in equation 1 is applied using MATLAB's *iterior point* minimisation algorithm. In table 2, the platform properties applied for the modelling of the LAPCAT A2 configuration are provided. An ultimate load factor of 2.5 is applied for the fuselage and wing structural mass computations and has been chosen according to the one previously used to model the LAPCAT A2 internal structure [17]. The emissivity used to calculate the convective heat transfers and TPS masses is set of 0.8 as recommended by [17]. A payload density of $50[kg/m^3]$ is used and has been set according the value of the 200 passenger horizontal take off hypersonic transports presented in HASA [7].

Table 2
Constant values associated with Baseline configuration

Property	Value	Unit
Number of Passengers	300	[-]
Fuel density (Liquid Hydrogen @1bar)	70.847	$[kg/m^3]$
Emissivity	0.8	[-]
Sub-structure temperature	400	[K]
Payload density	50	[kg/mˆ{3}]
Ultimate Load factor	2.5	[-]
Tank density (Liquid Hydrogen)	8.49	$[kg/m^3]$
Number of mission plateaux defined	9	[–]
Number of Fuselage cross sections	30 (equispaced)	[-]

In addition, the main settings applied for the calculations of the platform are given in table 3. The fuel is stored in the fuselage body and is fixed to start and end at 9.3% and 91% of the fuselage length according to the baseline configuration. The TPS type chosen in the platform is the silica based aerogel SiO_2TiO_2 for its thermal performance where the tps unit mass to heat load correlation is given according to figure 14 as given in section 2.4.2. An aluminium load bearing substructure is selected with a temperature of 400 Kelvins (TPS back wall temperature constrain). For the hypersonic inviscid flow analysis ($M_{inf} > 3$), the inclined wedge method is used for the wing and the interpolated Taylor Maccoll tangent-cone method is employed for the fuselage body. These methods have been selected since they provide the best estimation of lift and drag coefficient as well as local pressure coefficient as a function of freestream mach number and angle of attack as was concluded from extensive validation of the aerodynamic solver. For the engine model, the liquid hydrogen Generic Hypersonic Aircraft engine model (GHAME) is utilised and was defined in section 2.4.1. The baseline LAPCAT A2 configuration possesses a 3% thick airfoil section [24]. The airfoil sections in the platform are modelled as biconvex airfoils.

Table 3
Modelling setting parameters for platform

Setting	Value
Input Mission	Given in figures 7 and 8 (see section **??**)
Viscous semi-empirical model	Eckert reference enthalpy
Transition model	Flow assumed turbulent over entire surface
Fuel storage	Fuselage
TPS type	SiO2TiO2
Sub-structure material	Aluminum
Hypersonic impact method (wing)	Inclined Wedge
Hypersonic impact method (fuselage)	Interpolated Taylor Maccoll
Fuel Type	Liquid Hydrogen (no oxidizer)
Engine type	GHAME
Wing Airfoil	Biconvex (3% thickness/chord ratio)
Fuselage cross sections	Circular

The mesh used for optimal sizing is displayed in figure 15 and has been selected from a mesh convergence study using the objective function value M_{TO} as convergence criteria. The resulting mesh provides a computational time of 3.13 minutes per objective evaluation making it feasible for optimisation purposes while providing an objective value close to the fully converged objective value (0.4% difference).

3.1 Effects of range on optimal sizing

To study the effects of mission range on the optimal sizing, the sizing algorithm developed in this thesis is used on the LAPCAT A2 configuration for five different mission ranges by applying a scaling factor to the cruise phase of the original mission (figures 7 and 8). The resulting optimally sized geometries and associated estimated mass distributions are provided in figure 19 and 16.

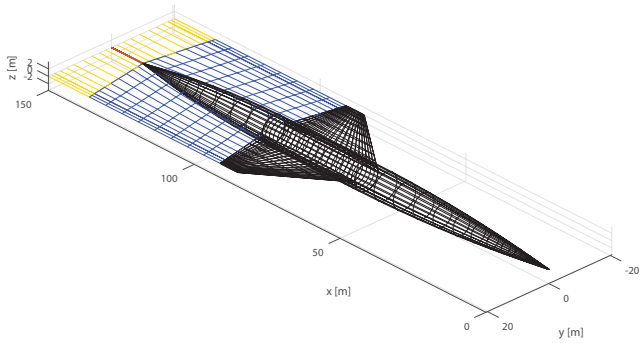

Fig. 15. LAPCAT A2 baseline configuration mesh chosen for optimisation.

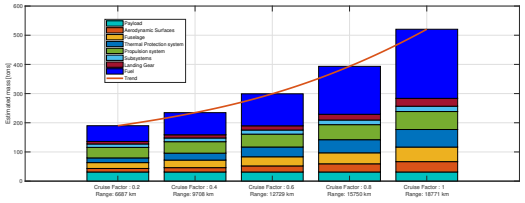

Fig. 16. Change in mass distribution of sized configurations with increasing range.

In figure 16 and table 5 the change in component and fuel mass for the different optimally sized configuration at varying cruise range is provided. From figure 16 it can be seen that the estimated take-off mass of the aircraft has shown to increase exponentially with linearly increasing mission range. The fuel mass has the highest growth rate with range thus leading to a reduction in empty mass to take-off mass ratio W_{emp}/W_{TO} from 72% to 54% at minimum and maximum range respectively. This fast growth in fuel mass relative to structural components is due to the combination of two factors. Firstly, as a result of the increase in distance, the fuel required to fly the additional range increases and secondly the snow ball effect further increases the fuel mass required. These effects leads to an exponential rise in fuel mass flow required to fly at further range as shown in figure 17. Associated with the exponential increase in fuel mass, the tank mass follows the same behaviour.

While the majority of structural components mass increases with respect to the aircraft mass through the snow effect, the thermal protection system mass mainly increases as a result of the increase in heat load due to the rising exposure time of the configuration in hypersonic cruise but is also a result of the increase in vehicle wetted area. The fuselage is the only structural compo-

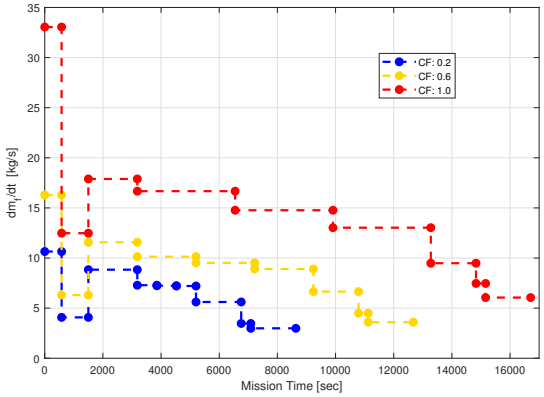

Fig. 17. Exponential rise in fuel mass flow with increasing range.

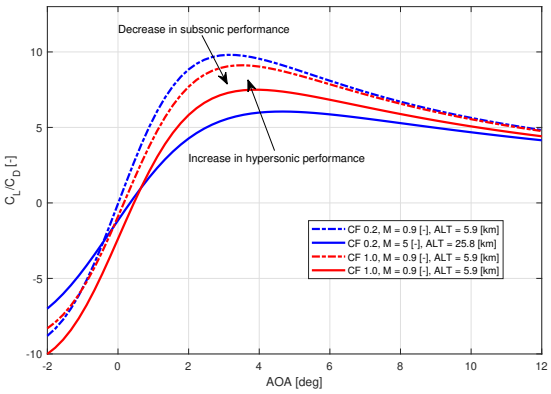

Fig. 18. Lift to drag ratio of optimised configurations for two different cruise factors.

nent which is not related to take-off mass according to the HASA weight estimation model but its mass still gradually increases as a result of the increased length of the body volume required to fit the liquid hydrogen fuel.

In table 4, the optimal design vector for the different mission ranges is provided. Although global minimum cannot be guaranteed since a local optimiser is used to size the configuration, some general trend can be observed in the design variables. The most noticeable change in design variable for varying cruise range is the aspect ratio which varies from a factor of 0.92 [-] at a cruise factor of 0.2 to a value of 0.58 [-] for the baseline mission (CF = 1). This change is believed to be due to the change in relative importance of subsonic aerodynamic performance as compared to hypersonic performance with increasing cruise factor. At a cruise factor of 0.2, subsonic conditions constitute a large portion of the mission profile whereby the aspect ratio shows a significant impact on subsonic lift to drag ratio. As a result the optimiser increases the aspect ratio at low cruise factors to ensure a good balance between subsonic and hypersonic aerodynamic performance. For higher cruise factor, the subsonic performance becomes less critical and the aspect ratio reduces to decrease the overall wing mass. The thickness to chord ratio on the other hand decreases with cruise factor to promote a reduction in hypersonic wave drag at the expense of an increase in wing mass. The difference in the optimal configuration lift to drag ratio for cruise factors of 0.2 and 1.0 is shown in figure 18. In this figure it can clearly be seen that as the cruise factor rises and the relative time spent in hypersonic cruise increases, the optimiser tries to maximise the hypersonic performance at the expense of a reduced subsonic lift to drag ratio. This behaviour clearly shows that the choice in optimal design is dependent on a compromise between subsonic and hypersonic flow regimes.

Other design variables such as the wing planform area increase proportionally to the increase in aircraft take-off mass with increasing range to ensure the configuration can generate sufficient lift. Additionally fuselage width and length factors also increase proportionally in order to fit the fuel required for the mission while fuselage height does not vary significantly. The fuselage length factor increases the most drastically with the increase in cruise factor (from 0.67 to 1.15) as it was observed to have the most beneficial effect on the hypersonic lift to drag ratio (through a reduction in wave drag and the generation of useful lift). It is important to note that for each of the sized configuration, the fuel volume is the limiting constrain thereby confirming that the fuel volume is one of the most critical constrains in the design of liquid hydrogen hypersonic transport aircraft.

Figure 20 presents a comparison between the Payload Range Efficiency (PRE) and payload mass fraction of the LAPCAT A2 configuration at varying range (as estimated using the developed platform) with other types of aircraft. The first aspect which is noticed regarding the performance estimation of the sized LAPCAT A2 configurations is that, with linearly increasing range, both PRE and payload fraction decrease significantly. The reduction in PRE with range for the LAPCAT A2 vehicle is believed to be a result of the exponential increase in fuel mass with linear increase in range which was previously observed in figure 16. Due to this exponential rise in required fuel mass, the payload mass fraction decreases proportionally as observed in figure 20. Regarding the comparison with other aircraft, the LAPCAT A2 is estimated to possess a lower PRE and payload fraction than typical kerosene subsonic aircraft (star symbol). This is mainly due to the higher lift to drag ratios which can be expected for subsonic aircraft (high fuel range efficiency) and due to the lower structural mass fraction of subsonic aircraft which do not require heavy liquid hydrogen tanks and Thermal protection systems. The LAPCAT A2 is however estimated to perform better than supersonic kerosene aircrafts (diamond) in terms of PRE which is mostly a result of the increased propulsive

Table 4
Optimal (normalised) design vector for sized aircraft at varying cruise factors

Design Variable	Unit	CF : 0.2 [-] Range: 6687 [km]	CF : 0.4 [-] Range: 9708 [km]	CF : 0.6 [-] Range: 12729 [km]	CF : 0.8 [-] Range: 15750 [km]	CF : 1.0 [-] Range: 18771 [km]
$F_{S_{wing}}$	[-]	0.47	0.60	0.87	1.12	1.59
$F_{wing,AR}$	[-]	0.92	0.87	0.80	0.74	0.58
$F_{wing,\lambda}$	[-]	0.78	0.59	0.59	0.26	1.00
$\epsilon_{tip,wing}$	[deg]	-0.08	-0.59	-0.12	-0.39	-1.00
$F_{(t/c)_{wing,airf}}$	[-]	0.98	0.92	0.87	0.74	0.75
$F_{fus,width}$	[-]	0.81	0.92	0.96	1.01	1.18
$F_{fus,height_{up}}$	[-]	0.59	0.52	0.60	0.84	0.70
$F_{fus,height_{lo}}$	[-]	0.71	0.67	0.70	0.68	0.79
$F_{fus,length}$	[-]	0.67	0.79	0.89	0.98	1.15

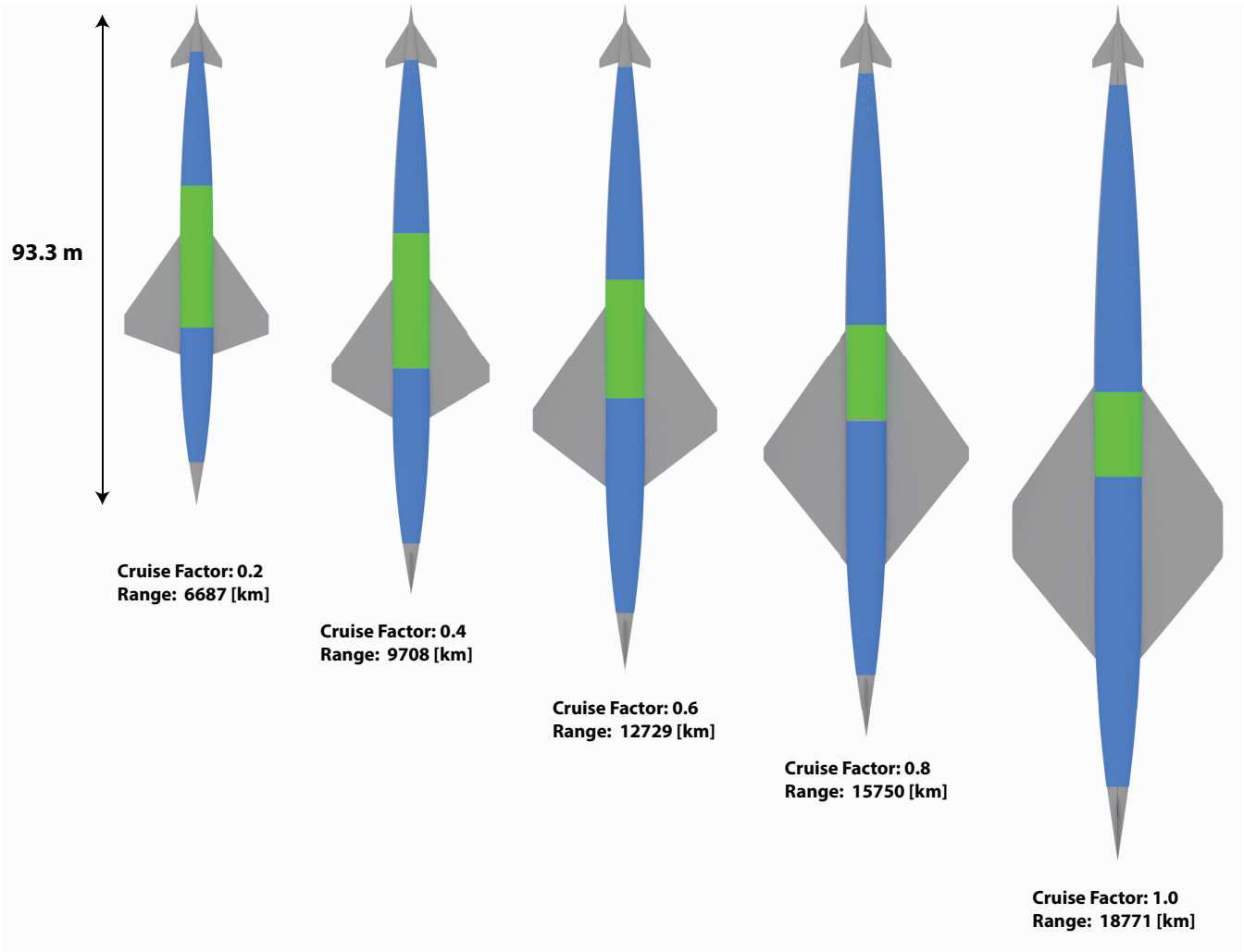

Fig. 19. Optimally sized configurations for varying mission range (top view).

efficiency of liquid hydrogen engines at high-speeds.

3.2 Effects of cruise mach number on baseline configuration

As a secondary study, the effects of the cruise mach number on the performance of the LAPCAT A2 baseline

Table 5
Estimated mass distribution for sized aircraft at varying cruise factors

Estimated Mass [tons]	**Sub-Component**	**CF : 0.2 [-]** **Range: 6687 [km]**	**CF : 0.4 [-]** **Range: 9708 [km]**	**CF : 0.6 [-]** **Range: 12729 [km]**	**CF : 0.8 [-]** **Range: 15750 [km]**	**CF : 1.0 [-]** **Range: 18771 [km]**
Payload		31.3	31.3	31.3	31.3	31.3
Aerodynamic Surfaces sub-total		12.0	14.9	20.8	28.0	35.5
	Main wing	*11.2*	*13.8*	*19.2*	*25.7*	*32.7*
	Vertical tail	*0.8*	*1.0*	*1.6*	*2.3*	*2.7*
Fuselage mass		20.1	25.9	31.3	37.6	49.9
Thermal protection system		16.1	23.7	33.5	45.0	60.1
Propulsion system sub-total		36.1	39.4	44.2	51.7	61.7
	Fuel tank structure	*6.5*	*9.1*	*13.3*	*19.8*	*28.4*
	Fuel tank insulation	*1.6*	*2.2*	*3.0*	*3.9*	*5.2*
	Engine Dry	*28.0*	*28.0*	*28.0*	*28.0*	*28.0*
Sub-system mass sub-total		11.7	12.7	14.1	15.9	18.2
	Electric sub-systems	*1.4*	*1.7*	*1.9*	*2.3*	*2.7*
	Hydro-Pneumatic sub-system	*0.6*	*0.7*	*0.8*	*0.9*	*1.1*
	Avionics	*3.2*	*3.5*	*3.8*	*4.2*	*4.6*
	Equipment	*6.4*	*6.9*	*7.5*	*8.5*	*9.7*
Landing gear		8.7	11.0	14.5	19.6	26.9
Operational Empty mass		136.0	158.9	189.7	229.2	283.7
Fuel mass		53.9	75.9	109.8	164.5	236.9
Take-off mass		190.0	234.7	299.5	393.6	520.6

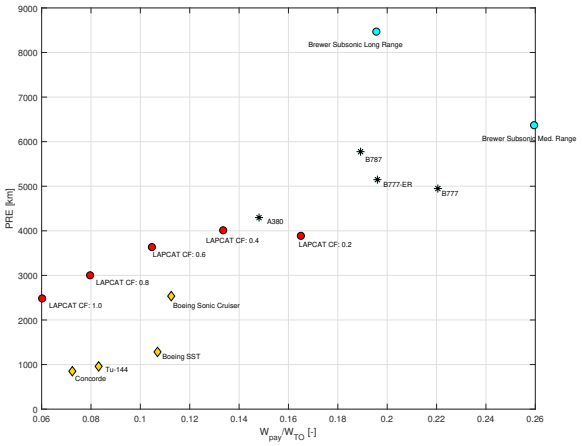

Fig. 20. Comparison of optimally sized configurations of the LAPCAT A2 vehicle with other aircraft.

configuration is investigated. In this study, the cruise mach number of the baseline mission is gradually increased while the mission time is scaled proportionally to allow for a fixed range of 18771 km.

With increasing mach numbers, the average heat transfer on the vehicle surface is calculated to increase at a near quadratic rate while temperatures vary near linearly for a fixed cruise altitude as can be observed in figures 21 and 22.

When looking at figure 23, the thermal protection system mass is predicted to gradually increase with higher cruise mach numbers for a fixed range. This is due to the observed quadratic increase in average convective heat transfer with increasing cruise mach numbers (figure 21). Since the convective heat transfer increases at a very high rate in comparison to the reduction in mission time that can be achieved when flying at a higher cruise mach number, the total heat transfer load over the vehicle rises with mach number thereby increasing the thermal protection system mass.

On the other hand, the decrease in mission time leads to a reduction in fuel mass. However at mach number higher than 7, the decrease in mission time cannot compensate for the reduction in engine specific impulse (figure 24) and increasing thermal protection mass. As a result, in terms of take-off mass, an increase in cruise mach number yeilds a reduction in mass for a fixed range due to the shorter flight times that can be achieved. However past a certain mach number the reduction in engine specific impulse and increase in thermal protection system mass cannot be compensated by the time reduction which leads to an optimum cruise mach number. In this case for the LAPCAT A2 baseline mission, the optimal mission mach number is estimated to be between mach 6 and 6.5. In general for an arbitrary configuration the optimum cruise mach number which minimises the aircraft take-off mass will thus mainly be dependent on a trade-off between mission time, engine specific impulse and thermal protection system mass.

4 Concluding remarks

The paper describes the implementation of a computationally efficient MDO platform for the optimal sizing of long-range hypersonic transport aircraft. Through the implementation of an efficient geometry (Engineering SketchPAD [5]) and mesh generator (SALOME [2])

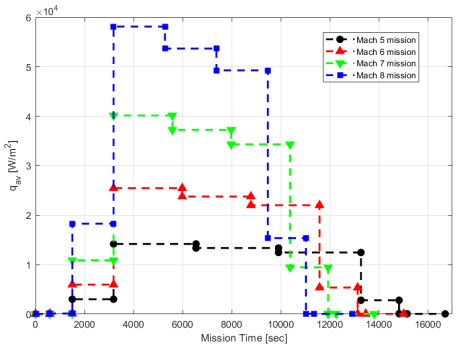

Fig. 21. Average convective heat transfer for mission with varying cruise mach number.

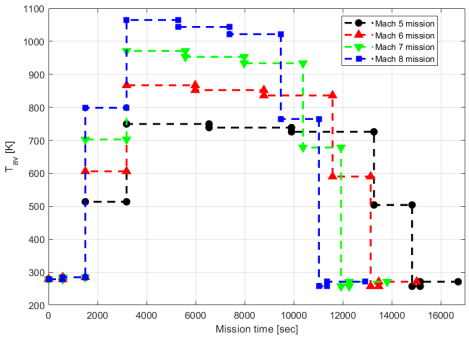

Fig. 22. Average conduction-radiation surface temperature for mission with varying cruise mach number.

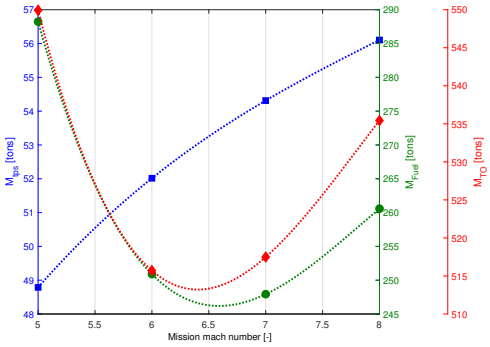

Fig. 23. Change in TPS, fuel and take-off mass for varying cruise mach numbers.

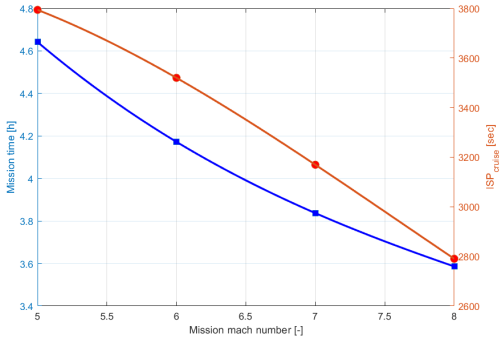

Fig. 24. Change in total mission time and cruise engine specific impulse for varying cruise mach numbers.

as well as low to medium fidelity aero-thermal solvers (PANAIR [20] and Hypersonic Engineering Methods), arbitrary wing-body configuration can be analysed allowing for the exploration of a large design space. With the discretisation of an input mission and generation of an aero-thermal performance matrix containing the main most important lift/drag performance as well as surface heat distribution (through the use of POD), the platform is capable of quickly estimating component and fuel mass breakdown of a complete configuration. The Multi-Discipline Feasible loop implemented uses a simple engine performance model (GHAME), derived parametric thermal protection functions and empirical based weight estimations to ensure fast convergence and consistency in aircraft estimated take-off mass.

Application of the platform for the optimal sizing of the LAPCAT A2 hypersonic transport configuration has shown the ability of the platform to size and estimate the mass of such vehicles at a conceptual design stage. Sizing of the configuration for varying range as shown that optimal aircraft wing and fuselage dimensions and shape can change drastically with range whereby the optimal design is mostly governed by fuel volume constrain and a trade-off between subsonic and hypersonic aerodynamic performance. Additionally, the clear exponential growth in take-off mass with range highlights one of the challenges of long-range hypersonic transport. Comparison of the performance of the LAPCAT A2 with other civil aviation aircraft has shown that while liquid hydrogen transport aircraft are not estimated to perform as well as subsonic kerosene and hydrogen aircraft in terms of Payload Range Efficiency and Payload mass fraction, the potential of liquid hydrogen propulsion allows such aircraft to outperform typical supersonic keresone aircraft in terms of PRE and provide time reductions which are unachievable by subsonic aircraft.

Investigation of the effect of cruise mach number on the LAPCAT A2 configuration for a fixed range has revealed the presence of an optimum cruise mach number for the minimisation of aircraft take-off mass. It has been shown that this optimum is dictated by a trade-off between thermal protection system mass which increases with mach number and fuel mass requirement which is mostly affected by mission time and engine specific impulse. Given the implemented platform ability to efficiently capture the critical design considerations for a

hypersonic transport and estimate the mass distribution of a complete configuration at an early design stage, the applied methodologies are believed to provide a strong basis for the implementation of MDO techniques in this field.

References

[1] Max L. Blosser* and Carl C. Poteet ** , Carl J. Martin* , Kamran Daryabeigi*. REUSABLE METALLIC THERMAL PROTECTION SYSTEMS DEVELOPMENT. *NASA Langley Research Center*.

[2] EDF. SALOME PLATFORM.

[3] George Emanuel. *Analytical Fluid Dynamics, Third Edition*. 2016.

[4] C. R. Glatt. WAATS A COMPUTER PROGRAM FOR WEIGHTS ANALYSIS OF ADVANCED TRANSPORTATION SYSTEMS. *Langley Research Center*, 2018.

[5] Robert Haimes. The Engineering Sketch Pad : A System for Building Parametric Geometry. (June):1–18, 2013.

[6] Robert Haimes and John F Dannenhoffer. The Engineering Sketch Pad : System for Building Parametric Geometry. pages 1–21.

[7] GARY J. HARLOFF and BRIAN M. BERKOWITZ. Hypersonic aerospace sizing analysis for the preliminary design of aerospace vehicles. *Journal of Aircraft*, 27(2):97–98, 1990.

[8] By Antonella Ingenito, Stefano Gulli, and Claudio Bruno. Preliminary Sizing of an Hypersonic Airbreathing Airliner. 8:19–28, 2010.

[9] Thomas Jazra and Michael Smart. Development of an Aerodynamics Code for the Optimisation of Hypersonic Vehicles. *47th AIAA Aerospace Sciences Meeting including The New Horizons Forum and Aerospace Exposition*, (January), 2009.

[10] Hiroaki Kobayashi, Hideyuki Taguchi, Exploration Agency, Takayuki Kojima, Exploration Agency, Tetsuya Sato, Senior Researcher, and Senior Researcher. Performance analysis of Mach 5 hypersonic turbojet. (September):1–9, 2012.

[11] Dietrich Rudolf Lampe. Thermally Perfect, Calorically Imperfect Taylor-Maccoll Flow. 9(5), 1994.

[12] Clare M. Lewandowski. A Computer Program for Predicting Subsonic or Supersonic Linear Potential Flows About Arbitrary Configurations Using A Higher Order Panel Method, Vol. I. Theory Document (Version 1.0). *The effects of brief mindfulness intervention on acute pain experience: An examination of individual difference*, 1, 2015.

[13] Jing Li and Weiwei Zhang. Theoretical & Applied Mechanics Letters The performance of proper orthogonal decomposition in discontinuous flows. *Theoretical & Applied Mechanics Letters*, 2016.

[14] Paula Margaretic, Rond-point Maurice Bellonte, and Blagnac Cedex. ECONOMICAL ASSESSMENT of COMMERCIAL HIGH- SPEED TRANSPORT. (112):1–30, 2015.

[15] Tadeusz J. Masternak. Multi-Objective Trajectory Optimization of a Hypersonic Reconnaissance Vehicle with Temperature Constraints. page 416, 2014.

[16] O.J. Murillo Jr. A fast ascent trajectory optimization method for hypersonic air-breathing vehicles. *Simulation*, page 140, 2010.

[17] Design Optimization and Long-range Hydrogen-fuelled Hypersonic Cruise Vehicles. Design Optimization and Analysis of Long-Range Hydrogen-Fuelled Hypersonic Cruise Vehicles. pages 2016–2017, 2017.

[18] PDAS. PANIN: Input Pre-Processor for PanAir. *Public Domain Aeronautical Software*.

[19] Jiri Polansky. Proper Orthogonal Decomposition as a technique for identifying multiphase flow regime based on Electrical Impedance Tomography. *University of Leeds*, 2015.

[20] Gary R. Saaris. A5021 User's Manual-PAN AIR Technology Program for Solving Problems o/Potential Flow about Arbitrary Configurations. *Boeing*, 1992.

[21] J Steelant. LAPCAT : High-Speed Propulsion Technology. pages 1–38, 2008.

[22] T H E Mark I V Supersonic-hypersonic, E Arvel, Douglas N Smyth, and Wayne R Oliver. Mark IV SuperHypersonic Arbitrary Body Program. II, 1973.

[23] Takeshi Tsuchiya, Yoichi Takenaka, and Hideyuki Taguchi. Multidisciplinary Design Optimization for Hypersonic Experimental Vehicle. *AIAA Journal*, 45(7):1655–1662, 2007.

[24] Dries Verstraete, Shayan Sharifzadeh, Patrick Hendrick, and Mechatronic Engineering. DEFINITION AND AERO-ELASTIC OPTIMISATION OF THE STRUCTURE OF THE LAPCAT A2 MACH 5 AIRLINER. 2006.

[25] R D Witcofski. HYDROGEN FUELED HYPERSONIC TRANSPORTS. *NASA Langley Research Center*.